AMERICAN SOCIETY FOR MICROBIOLOGY | Journal of Virology

BPIFB6 Regulates Secretory Pathway Trafficking and Enterovirus Replication

Stefanie Morosky, Nicholas J. Lennemann, Carolyn B. Coyne

Department of Microbiology and Molecular Genetics, University of Pittsburgh, Pittsburgh, Pennsylvania, USA

ABSTRACT

Bactericidal/permeability-increasing protein (BPI) fold-containing family B, member 3 (BPIFB3) is an endoplasmic reticulum (ER)-localized host factor that negatively regulates coxsackievirus B (CVB) replication through its control of the autophagic pathway. Here, we show that another member of the BPIFB family, BPIFB6, functions as a positive regulator of CVB, and other enterovirus, replication by controlling secretory pathway trafficking and Golgi complex morphology. We show that similar to BPIFB3, BPIFB6 localizes exclusively to the ER, where it associates with other members of the BPIFB family. However, in contrast to our findings that RNA interference (RNAi)-mediated silencing of BPIFB3 greatly enhances CVB replication, we show that silencing of BPIFB6 expression dramatically suppresses enterovirus replication in a pan-viral manner. Mechanistically, we show that loss of BPIFB6 expression induces pronounced alterations in retrograde and anterograde trafficking, which correlate with dramatic fragmentation of the Golgi complex. Taken together, these data implicate BPIFB6 as a key regulator of secretory pathway trafficking and viral replication and suggest that members of the BPIFB family participate in diverse host cell functions to regulate virus infections.

IMPORTANCE

Enterovirus infections are associated with a number of severe pathologies, such as aseptic meningitis, dilated cardiomyopathy, type I diabetes, paralysis, and even death. These viruses, which include coxsackievirus B (CVB), poliovirus (PV), and enterovirus 71 (EV71), co-opt the host cell secretory pathway, which controls the transport of proteins from the endoplasmic reticulum to the Golgi complex, to facilitate their replication. Here we report on the identification of a novel regulator of the secretory pathway, bactericidal/permeability-increasing protein (BPI) fold-containing family B, member 6 (BPIFB6), whose expression is required for enterovirus replication. We show that loss of BPIFB6 expression correlates with pronounced defects in the secretory pathway and greatly reduces the replication of CVB, PV, and EV71. Our results thus identify a novel host cell therapeutic target whose function could be targeted to alter enterovirus replication.

Transport of cargo from the endoplasmic reticulum (ER) to the Golgi complex requires a highly controlled system of proteins that function to regulate a variety of steps along the secretory pathway. These components must not only synchronize the loading of diverse cargo but also navigate the trafficking of this cargo to specific cellular compartments. The Golgi complex functions as a focal point of secretory pathway trafficking as it controls not only the anterograde trafficking of newly synthesized proteins from the ER to the cell membrane but also must facilitate the retrograde trafficking of surface-associated molecules from the plasma membrane back to the ER. Vesicles trafficking along the secretory pathway target their cargo to the Golgi complex via the use of distinct tethering machinery, such as the conserved oligomeric Golgi (COG) complex, whose members function to anchor coat protein (COPI)-coated retrograde vesicles to the Golgi complex by interacting with a variety of Rab GTPases, SNAREs, and components of COPI vesicles (1–6). Mutations in the COG complex (1, 5, 7, 8), depletion of COG complex components by RNA interference (RNAi) (9), or genetic mutations (8) induce dramatic alterations in Golgi complex function and morphology.

In addition to its important function in maintaining cellular homeostasis, the secretory pathway is also targeted by viruses to facilitate various aspects of their replicative life cycles. An obligate step in the life cycle of positive-sense RNA viruses is the formation of membrane-enriched organelles that provide the structural foundation for viral replication. These organelles are often derived from the host cell secretory pathway and are formed by specific virally encoded proteins that enrich these structures with the necessary lipid and protein components to optimize replication. Enteroviruses, which belong to the *Picornaviridae* family, rely on both protein and lipid components of the secretory pathway to provide the structural scaffolding for their replication. The importance of the secretory pathway in enterovirus replication is underscored by the extreme sensitivity of these viruses to brefeldin A (BFA), a potent inhibitor of the secretory pathway that induces Golgi complex disassembly and ER accumulation of secretory proteins (10, 11). Enteroviruses encode several proteins that directly target secretory pathway-associated molecules, such as the virally encoded 3A protein, which disrupts ER-to-Golgi transport and induces the disassembly of the ER-Golgi intermediate compartment (ERGIC) (12, 13), and the 2B integral membrane protein, which localizes primarily to the Golgi complex and partially

Received 27 January 2016 **Accepted** 6 March 2016

Accepted manuscript posted online 9 March 2016

Citation Morosky S, Lennemann NJ, Coyne CB. 2016. BPIFB6 regulates secretory pathway trafficking and enterovirus replication. J Virol 90:5098–5107. doi:10.1128/JVI.00170-16.

Editor: D. S. Lyles

Address correspondence to Carolyn Coyne, coynec2@pitt.edu.

to the ER, where it enhances ion flux from both compartments in order to inhibit secretory pathway trafficking (14).

Previously, we identified bactericidal/permeability-increasing protein (BPI) fold-containing family B, member 3 (BPIFB3; also known as long palate, lung, and nasal epithelium clone [LPLUNC3]), as a host factor involved in regulating infection of the enterovirus coxsackievirus B (CVB) through its control of the autophagic pathway (15). In contrast, BPIFB3 silencing had no effect on the replication of the related enterovirus poliovirus (PV), suggesting that BPIFB3 functions in a virus-specific manner. BPIFB3 is a member of the BPI and lipopolysaccharide-binding protein (LBP) family of secreted antibacterial components, which also includes BPIFB1, BPIFB2, BPIFB4, and BPIFB6 (16). However, our previous work showed that BPIFB3 is not secreted and is localized exclusively to the ER (15). Members of the BPIFB family share sequence homology with cholesterylester transfer protein (CETP) and phospholipid transfer protein (PLTP), both of which are involved in lipid transport in plasma (17), but the physiological functions of the BPIFB family remain largely unknown. Here we show that in contrast to our previous findings with BPIFB3, silencing of BPIFB6 suppresses enterovirus replication in a panviral manner. In addition, we show that similar to BPIFB3, BPIFB6 localizes specifically to the ER, where it interacts with BPIFB3. However, unlike BPIFB3, which negatively regulates CVB replication through autophagy (15), we show that BPIFB6 regulates secretory pathway trafficking and its RNAi-mediated depletion disrupts both anterograde and retrograde trafficking and induces pronounced Golgi complex fragmentation. Our work thus identifies specific members of the BPIFB family as regulators of enterovirus replication via their control of distinct host cell pathways.

MATERIALS AND METHODS

Cells and viruses. Experiments were conducted using human brain microvascular endothelial cells (HBMECs), cultured as described previously (18), unless stated otherwise. HEK293T, HeLa, and U2OS cells were cultured in Dulbecco's modified Eagle's medium (DMEM) containing 10% fetal bovine serum and penicillin-streptomycin. Experiments were performed with coxsackievirus B3 (CVB3)-RD or PV (Sabin type I), expanded as described previously (19, 20). Echovirus 11 (E11 [Gregory strain]) and enterovirus 71 (EV71 [BrCr]) were purchased from the ATCC. Cells were infected with 1 to 3 PFU/cell (CVB, PV, and E11) or 5 PFU/cell (EV71) for ~16 to 18 h. Plaque assays were performed as described previously (19, 21). CellLight ER-RFP BacMam 2.0 baculovirus was purchased from Invitrogen.

Plasmids, siRNAs, and transfections. Flag-tagged BPIFB3 and V5-tagged BPIFB6 were described previously (15). V5-tagged BPIFB2 and BPIFB4 were generated by amplification of BPIFB2 or BPIFB4 cDNA following by cloning into pcDNA3.1/V5-His TOPO TA as per the manufacturer's instructions (Invitrogen). Green fluorescent protein (GFP)-fused Sec61β was generated by amplification of Sec61β cDNA following by cloning into pcDNA3.1/NT-GFP-TOPO as per the manufacturer's instructions (Invitrogen). GFP-tagged atlastin-3 (ATL3) and mCherry-tagged CLIMP63 were kindly provided by Gia Voeltz (University of Colorado). Small interfering RNAs (siRNAs) targeting BPIFB2 to -6 have been described previously (15). The sequences of the siRNAs targeting COG3 and COG7 are as follows: COG3si, AGACUUGUGCAGUUUAAC Att; and COG7si, AUCAGUCCAAAGUGUUUGUtt. All siRNAs were purchased from Sigma. Control (scrambled) siRNA was also purchased from Sigma.

Plasmid transfections were performed using X-tremeGENE 9 (Roche) essentially per the manufacturer's protocol. For siRNA transfections, cells were reverse transfected with siRNAs (final concentration, 25 to 50 nM) using DharmaFECT-1 transfection reagent (Thermo-Fisher Scientific) according to the manufacturer's protocol.

Antibodies. Rabbit polyclonal and mouse monoclonal antibodies directed against GFP (FL), Flag/OctA (D-8, H-5), GAPDH (glyceraldehyde-3-phosphate dehydrogenase) (FL-335), and His tag (H-15), were purchased from Santa Cruz Biotechnology. Mouse monoclonal anti-Flag (M2) and rabbit polyclonal anti-BPIFB6 were purchased from Sigma. Mouse anti-V5 was purchased from Invitrogen. Mouse anti-double-stranded RNA (anti-dsRNA) (J2) antibody was purchased from Scicons. Mouse monoclonal antibodies to Sec31A, p230/Golgin, GM130, GS15, and GS28 were purchased from BD Biosciences. Rabbit polyclonal βCOP was purchased from Novus Biologicals. Mouse anti-enterovirus VP1 (Ncl-Entero) was obtained from Novocastra Laboratories. Alexa Fluor-conjugated secondary antibodies were purchased from Invitrogen.

Immunofluorescence and electron microscopy. Cells cultured in chamber slides (LabTek; Nunc) were washed and fixed with 4% paraformaldehyde (PFA) and were then permeabilized with 0.1 to 0.25% Triton X-100 in phosphate-buffered saline (PBS) and incubated with the indicated primary antibodies for 1 h at room temperature. Following washing, cells were incubated with secondary antibodies for 30 min at room temperature, washed, and mounted with Vectashield (Vector Laboratories) containing 4′,6-diamidino-2-phenylindole (DAPI). The technique utilized for digitonin/Triton X-100 staining was performed as described previously (22). Images were captured using an FV1000 confocal laser scanning microscope (Olympus), analyzed using Imaris (Bitplane), and contrasted and merged using Photoshop (Adobe). Electron microscopy was performed as described previously (21).

Immunoblotting and immunoprecipitations. Cell lysates were prepared with radioimmunoprecipitation assay (RIPA) buffer (50 mM Tris-HCl [pH 7.4]; 1% NP-40; 0.25% sodium deoxycholate; 150 mM NaCl; 1 mM EDTA; 1 mM phenylmethanesulfonyl fluoride; 1 mg/ml aprotinin, leupeptin, and pepstatin; 1 mM sodium orthovanadate). Lysates (30 μg) were loaded onto 4 to 20% Tris-HCl gels (Bio-Rad, Hercules, CA) and transferred to nitrocellulose membranes. Membranes were blocked in 5% nonfat dry milk, probed with the indicated antibodies, and developed with horseradish peroxidase (HRP)-conjugated secondary antibodies (Santa Cruz Biotechology) and SuperSignal West Pico or West Dura chemiluminescent substrates (Pierce Biotechnology).

For immunoprecipitations, HEK293T cells transfected with the indicated plasmids were lysed with EBC buffer (0.5% NP-40, 50 mM Tris-HCl, 120 mM NaCl, 5 mM EDTA [pH 8.0]), and insoluble material was cleared by centrifugation. Lysates were incubated with the indicated antibodies for 1 to 2 h at 4°C followed by the addition of Sepharose G beads for an additional 1 to 2 h at 4°C. After centrifugation, the beads were washed with NETN lysis buffer (0.5% NP-40, 900 mM NaCl, 20 mM Tris, 1 mM EDTA) a minimum of five times and heated at 95°C for 10 min in Laemmli sample buffer. Following a brief centrifugation, the supernatant was immunoblotted with the indicated antibodies as described above.

Recombinant protein purification and lipid dot blots. The individual BPI domains of BPIFB3 and BPIFB6 were amplified from cDNA and cloned into the Champion pET-SUMO expression system as per the manufacturer's instructions (Invitrogen). This system generates the expression of recombinant proteins with N-terminal 6×His tags and SUMO fusion proteins. To generate recombinant proteins, plasmids were transformed into BL21(DE3) cells, and overnight cultures were treated with 1 mM isopropyl-β-D-thiogalactopyranoside (IPTG) while in the mid-log phase of growth. Cultures were incubated for another 2 h at 37°C with shaking, and the cells were collected by centrifugation. Recombinant proteins were purified using an Ni-nitrilotriacetic acid (NTA) purification system (Thermo Fisher) and concentrated with a polyethersulfone membrane concentrator (Pierce) as per the manufacturer's instructions. The purity of SUMO-conjugated fusion proteins was assessed using SDS-PAGE followed by Coomassie staining or immunoblotting with anti-6×His antibody. Protein concentrations were determined by bicinchoninic acid (BCA) protein assay.

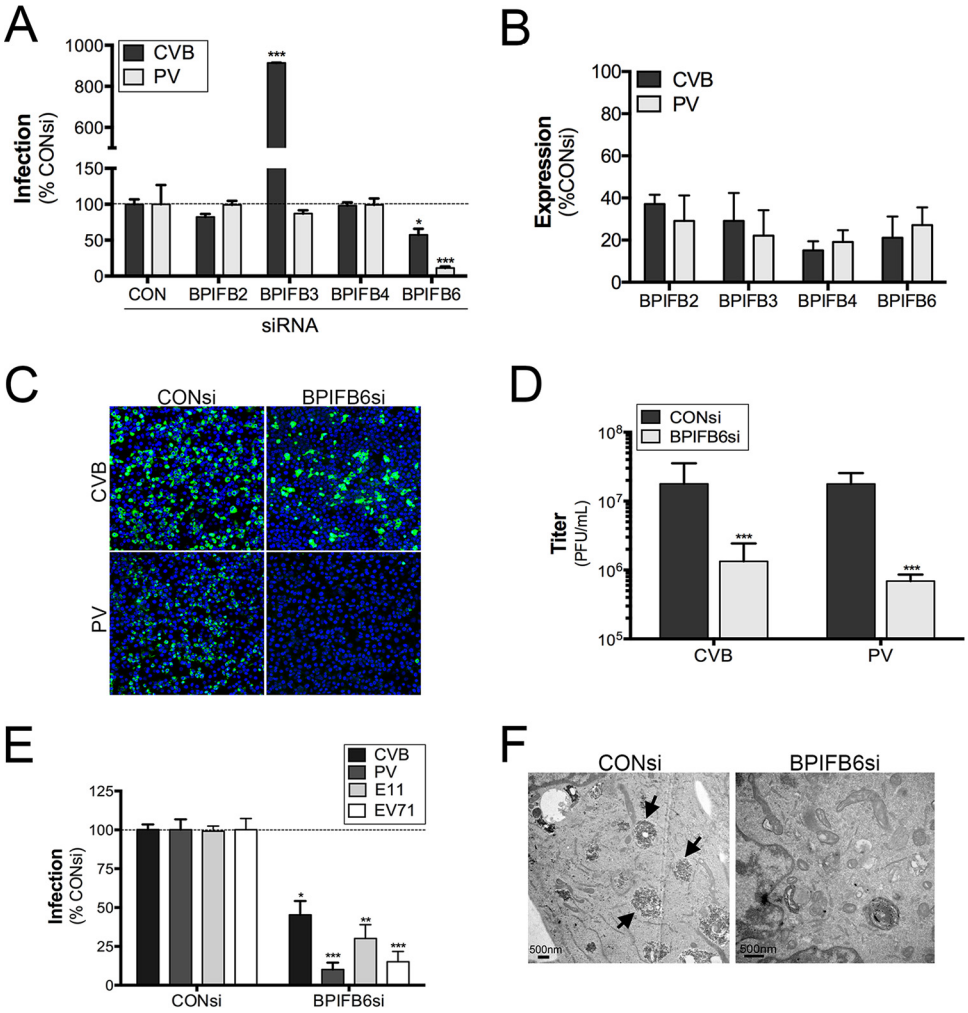

FIG 1 Enterovirus replication is suppressed by silencing of BPIFB6. (A) HBMECs were transfected with siRNAs against BPIFB2, BPIFB3, BPIFB4, and BPIFB6 and infected with CVB (3 PFU/cell) or PV (1 PFU/cell) ~48 h later. Infections were quantified by RT-qPCR. Data are shown as a percentage of change from the control (CONsi [scrambled]) siRNA. (B) RT-qPCR for expression of the indicated BPIFB family members from samples shown in panel A. Data are shown as a percentage of change from the control (scrambled). (C) Immunofluorescence microscopy for CVB (top row) or PV (bottom row) viral RNA (vRNA) (using anti-dsRNA J2 antibody [green]) in cells transfected with CONsi or BPIFB6si. (D) CVB and PV titers (shown as PFU per milliliter) in cells transfected with CONsi or BPIFB6si. (E) HBMECs were transfected with CONsi or BPIFB6si and infected with CVB, PV, E11, or EV71 ~48 h later. Infections were quantified by RT-qPCR. Data are shown as a percentage of change from CONsi. (F) Transmission electron micrographs of HBMECs transfected with CONsi or BPIFB6si and infected with CVB (3 PFU/cell) for ~16 h. Black arrows denote virus-filled replication organelles in CONsi-transfected cells that are absent in BPIFB6si-transfected cells. The scale bar at the bottom left is 500 nm. In panels A and B and D and E, data are shown as means ± standard deviations (*, $P < 0.01$; **, $P < 0.05$; ***, $P < 0.001$).

Lipid dot blots were performed using the indicated SUMO-6×His-tagged BPI domains isolated as described above and membrane lipid strips (Echelon). Lipid strips were incubated in blocking buffer (PBS-T: PBS containing 0.1% Tween 20 and 3% bovine serum albumin [BSA]) for 1 h at room temperature. Following washing with PBS-T, strips were incubated with 0.5 μg/ml of purified SUMO-6×His-tagged BPI domains in PBS-T containing 3% BSA for 1 h at room temperature. Following washing, membranes were incubated with anti-6×His-HRP antibody in PBS-T containing 3% BSA for 1 h at room temperature, washed, and then developed using West Dura chemiluminescent substrates (Pierce Biotechnology).

RT-qPCR. Total RNA was extracted using TRI reagent (MRC) according to the manufacturer's protocol or using GenElute mammalian total RNA miniprep kits (Sigma). RNA samples were treated with RNase-free DNase (Sigma). Total RNA was reverse transcribed using the iScript cDNA synthesis kit (Bio-Rad, Hercules, CA). For each sample, 1 μg RNA was used for cDNA synthesis. Reverse transcription-quantitative PCR (RT-qPCR) was performed using iQ SYBR green supermix (Bio-Rad) in an Applied Biosystems StepOnePlus real-time PCR machine. Gene expression was calculated using the $2^{-\Delta\Delta CT}$ threshold cycle method (23), normalized to human β-actin. Primers against BPIFB2 to -6, actin, CVB, and PV have been described elsewhere (15, 21). The sequences of the primers against COG3 and COG7 are as follows: COG3, 5′-AGACAGATGAGGGATTACTTG-3′ and 5′-TAGGGTTCCTGTCTTATTGG-3′; and COG7, 5′-AGTCCAAAGTGTTTGTGAAG-3′ and 5′-CCTTGTGACACTTGTAGTAG-3′. The sequences of the primers against E11 are as follows: 5′-CGCTATGGCTACGGGTAAAT-3′ and 5′-GCAGTCCAACATCCCAGATAA-3′.

Statistical analysis. Data are presented as means ± standard deviations unless otherwise stated and were analyzed with Prism software (Graphpad) by two-tailed unpaired Student's *t* test. All experiments were performed a minimum of three times.

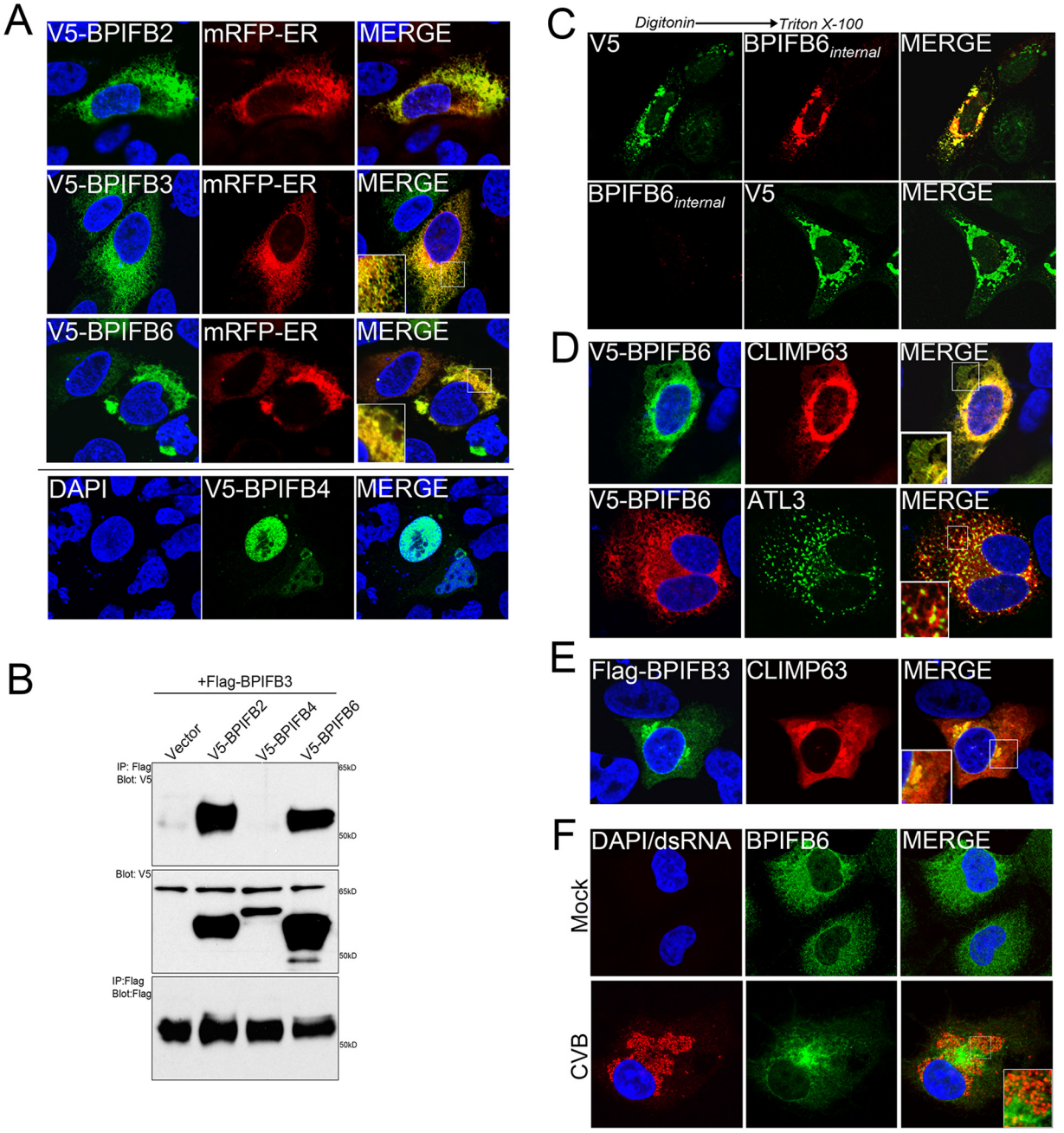

FIG 2 BPIFB6 localizes to the ER and interacts with BPIFB3. (A, top) Confocal microscopy for V5 (green) and ER-mRFP (red) in U2OS cells transfected with V5-BPIFB2, -BPIFB3, and -BPIFB6 and infected with CellLights ER-RFP baculovirus. At bottom left is an ~2× magnification of the area indicated by the white box in the merged image. (A, bottom) U2OS cells transfected with V5-BPIFB4 (green). (B) Coimmunoprecipitations for Flag-BPIFB3 and V5-BPIFB2, -BPIFB4, or –BPIFB6 in 293T cells transiently transfected with the indicated constructs (or vector control). Lysates were subjected to immunoprecipitation (IP) of Flag-BPIFB3 (using agarose bead-conjugated anti-Flag OctA), and immunoprecipitates were subjected to immunoblotting for V5 (top row) or Flag (bottom row). Whole-cell lysates were collected and immunoblotted for V5 (middle panel) to control for transfection efficiency of V5-fused BPIFB members. (C) Confocal microscopy of U2OS cells transiently transfected with V5-BPIFB6. Posttransfection (~48 h), cells were permeabilized with digitonin, fixed with paraformaldehyde (PFA), and then incubated with anti-V5 antibody (top row) or BPIFB6 (bottom row) antibodies. Cells were then permeabilized with Triton X-100 and stained with anti-BPIFB6 (top row) or anti-V5 (bottom row) antibodies. (D) Confocal microscopy for V5-BPIFB6 (top row, green; bottom row, red) and either mCherry-CLIMP63 (top row, red) or enhanced green fluorescent protein (EGFP)-ATL3 (bottom row, green) in transiently transfected U2OS cells. (E) Confocal microscopy for Flag-BPIFB3 (green) and mCherry-CLIMP63 (red) in transiently transfected U2OS cells. (F) Confocal microscopy for endogenous BPIFB6 (green) and CVB dsRNA (red) in mock- or CVB-infected (1 PFU/cell for ~16 h) HBMECs. Panels D to F contain a magnified image of the area shown in the white box. In panels A and C to F, DAPI-stained nuclei are shown in blue.

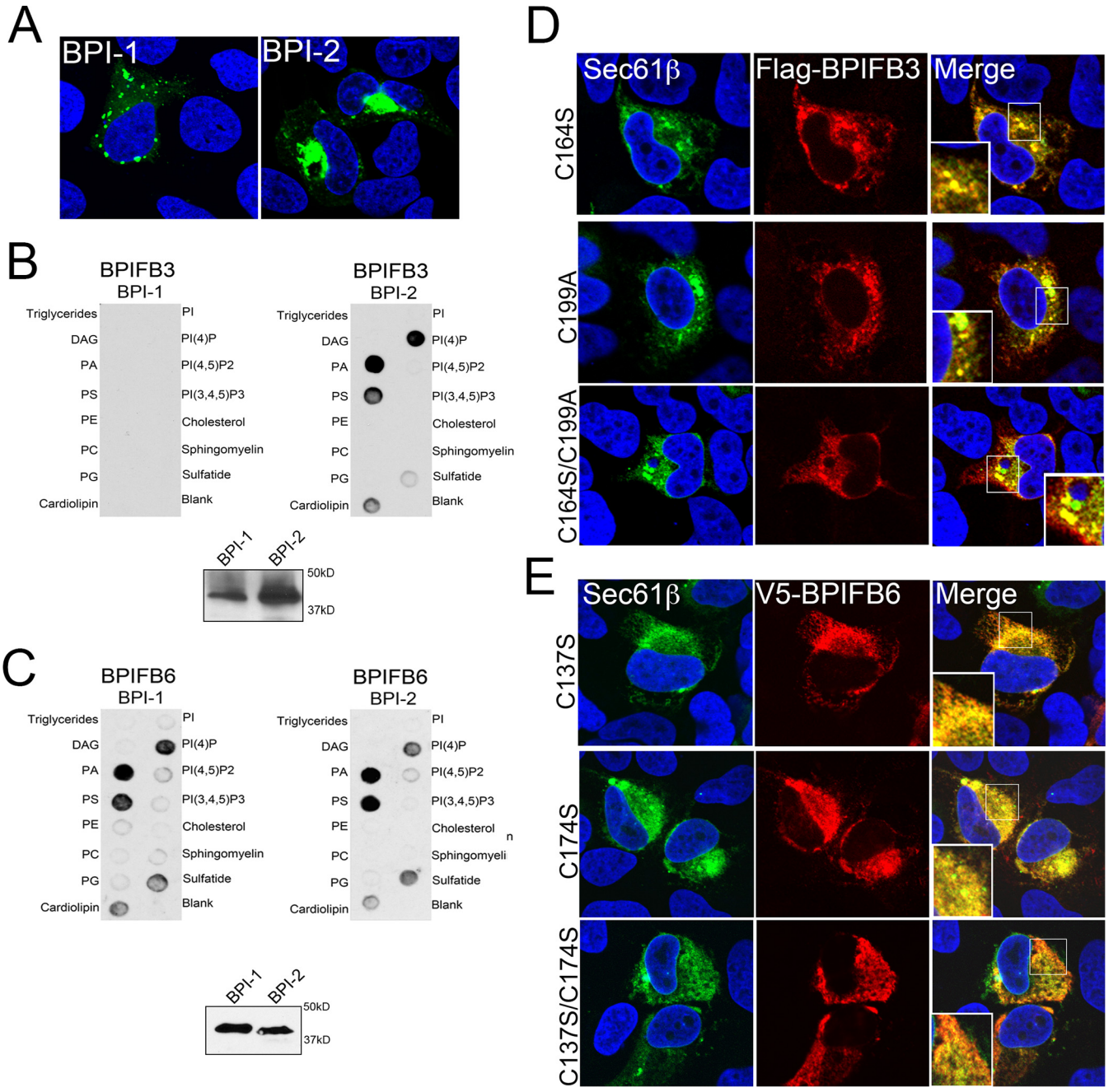

FIG 3 BPIFB6 localizes to the ER and interacts with BPIFB3. (A) Confocal microscopy for EGFP-fused BPI domains of BPIFB6. (B and C) Lipid dot blots using purified 6×His-tagged recombinant BPI domains of BPIFB3 (B) or BPIFB6 (C). At bottom are shown immunoblots (using anti-6×His antibody) for purified BPI domains of BPIFB3 (B) or BPIFB6 (C). (D and E) Confocal microscopy for Flag (red [D]) or V5 (red [E]) and EGFP-Sec61β (green [D and E]) in U2OS cells transfected with the wild type or the indicated lipid binding mutants of Flag-BPIFB3 (D) or V5-BPIFB6 (E). At bottom left is shown an ~2× magnification of the area indicated by the white box in the merged image. In both panels D and E, DAPI-stained nuclei are in blue.

RESULTS

RNAi-mediated silencing of BPIFB6 restricts enterovirus replication. Previously, we showed that RNAi-mediated silencing of BPIFB3 enhanced CVB, but not PV, replication (15). In contrast, whereas silencing of other members of the BPIFB family, such as BPIFB2 and BPIFB4, had no effect on either CVB or PV replication, silencing of BPIFB6 significantly reduced the levels of CVB and PV viral RNA (vRNA) (Fig. 1A and C) (15) and led to a >1-log loss of CVB and PV infectious titers (Fig. 1D). Knockdown efficiency was confirmed by RT-qPCR (Fig. 1B).

Although silencing of BPIFB3 substantially increases CVB replication, it has no impact on PV replication (15), suggesting that this member of the BPIFB family exerts its effects on enterovirus replication in a virus-specific manner. To determine if the effect of BPIFB6 silencing also exerted similar virus-specific effects, we profiled the effects of silencing BPIFB6 on CVB, PV, echovirus 11

(E11), and enterovirus 71 (EV71) replication and found that in all cases, knockdown of BPIFB6 expression significantly reduced viral replication (Fig. 1E). The inhibition of viral replication occurred prior to the formation of viral replication organelles as we did not observe the formation of replication organelles in CVB-infected cells transfected with BPIFB6 siRNA (Fig. 1F). Taken together, these data identify BPIFB6 as a positive regulator in the replication of enteroviruses from several species groups.

BPIFB6 localizes to the ER and interacts with BPIFB2 and BPIFB3. We found previously that BPIFB3 specifically localizes to the ER (15). To profile the localization of BPIFB6 and other members of the BPIFB family, we performed immunofluorescence microscopy for V5-tagged BPIFB2, BPIFB3, BPIFB4, and BPIFB6 with an ER-specific marker. We found that like BPIFB3, BPIFB2 and BPIFB6 localized to the ER and exhibited pronounced colocalization with the ER-specific marker monomeric red fluorescent protein (mRFP-ER) (Fig. 2A). In contrast, we found that BPIFB4 localized almost exclusively to the nucleus (Fig. 2A). Interestingly, silencing of BPIFB4 exerted no effects on either CVB or PV replication (Fig. 1A) (15).

We next determined whether members of the BPIFB family interact (either directly or indirectly) by performing coimmunoprecipitation studies. We found that BPIFB3 interacted with both BPIFB2 and BPIFB6, but not with BPIFB4, consistent with its localization in the nucleus, (Fig. 2B). Given that BPIFB4 localizes to the nucleus, whereas BPIFB2, BPIFB3, and BPIFB6 localize to the ER, these results suggest that select members of the BPIFB family may form a complex in the ER.

To determine the topology of BPIFB6 within the ER, we applied an immunostaining technique that involves a two-step permeabilization procedure utilizing digitonin to first permeabilize the plasma membrane, followed by Triton X-100 to permeabilize intracellular membranes (22), and which we previously used for BPIFB3 (15). We found that the V5-fused C-terminal domain of BPIFB6 (recognized by anti-V5 antibody) was located in the cytosol and was readily detectable by digitonin permeabilization alone (Fig. 2C, top row), whereas an internal region of BPIFB6 (detected by an antibody recognizing the second BPI domain) was localized within the ER lumen and required Triton X-100 permeabilization for its detection, suggesting this region of the protein is masked by the ER membrane (Fig. 2C, bottom row). Interestingly, none of the BPIFB family members are predicted to contain a transmembrane domain.

The ER exists as a network of sheets and tubules, which differ in their extent of membrane curvature and exhibit differential patterns of protein localization. We next determined whether BPIFB6 exhibited a specific pattern of localization to these distinct ER domains by performing localization studies with ER-associated proteins exhibiting specific localization to ER sheets or tubules. We found that BPIFB6 localized primarily to ER sheets, as determined by its strong colocalization with CLIMP63, a coiled-coil domain-containing protein that specifically localizes to ER sheets (24). In contrast, BPIFB6 did not exhibit any localization with atlastin-3 (ATL3), which localizes to three-way junctions of ER tubules (25) (Fig. 2D). Unlike BPIFB6, we found that BPIFB3 exhibited less significant association with CLIMP63, suggesting that it associates less with ER sheets (Fig. 2E). Finally, we found that CVB infection induced the reorganization of BPIFB6, but that BPIFB6 did not colocalize with viral dsRNA in replication organelles (Fig. 2F).

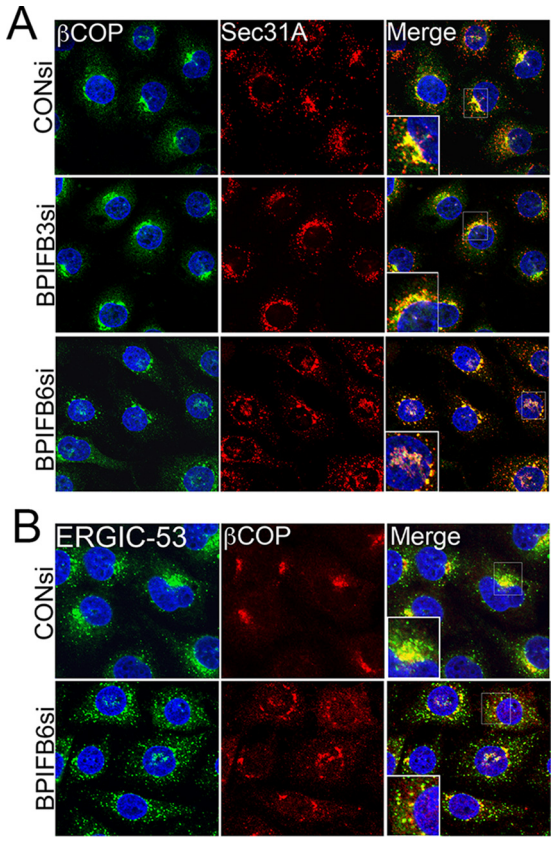

FIG 4 Silencing of BPIFB6 disrupts retrograde and anterograde trafficking. (A) Confocal microscopy for βCOP (green) and Sec31A (red) in HBMECs transfected with control siRNA (scrambled [CONsi]), BPIFB3si, or BPIFB6si. (B) Confocal microscopy for ERGIC-53 (green) and βCOP (red) in HBMECs transfected with CONsi or BPIFB6si.

Lipid binding properties of the BPI domains of BPIFB6. Although members of the BPIFB family share sequence homology with the lipid transporters CETP and PLTP (17), their lipid binding properties have not been characterized. Similar to BPIFB3 (15), we found that the individual BPI domains of BPIFB6 localized to the cytoplasm (Fig. 3A). To compare the specific lipids that the BPI domains of BPIFB3 and BPIFB6 bind, we generated recombinant 6×His-tagged proteins of both BPI domains of BPIFB3 and BPIFB6 and tested their specific abilities to bind lipids by a lipid dot blot assay. We found that the second BPI domain of BPIFB3 (BPI-2) as well as both BPI domains of BPIFB6 (BPI-1 and BPI-2) specifically associated with phosphatidic acid (PA), phosphatidylserine (PS), and phosphatidylinositol (4)-phosphate [PI(4)P], and to a lesser extent to cardiolipin and 3-sulfogalactosylceramide (sulfatide) (Fig. 3B and C).

We next assessed whether the lipid binding properties of BPIFB3 and BPIFB6 were responsible for their localization to the ER. To do this, we performed site-directed mutagenesis of cysteine residues located within the BPI-1 domains of BPIFB3 and BPIFB6 that are predicted to form a disulfide bond based upon the conservation of these sites with the lipid-binding proteins BPI, lipopolysaccharide (LPS)-binding protein (LBP), CETP, and PLTP (26, 27). Disulfide bond formation is critical for the lipid binding activity of BPI (27). We generated both single and double mutations of these sites and assessed the ability of these mutants to

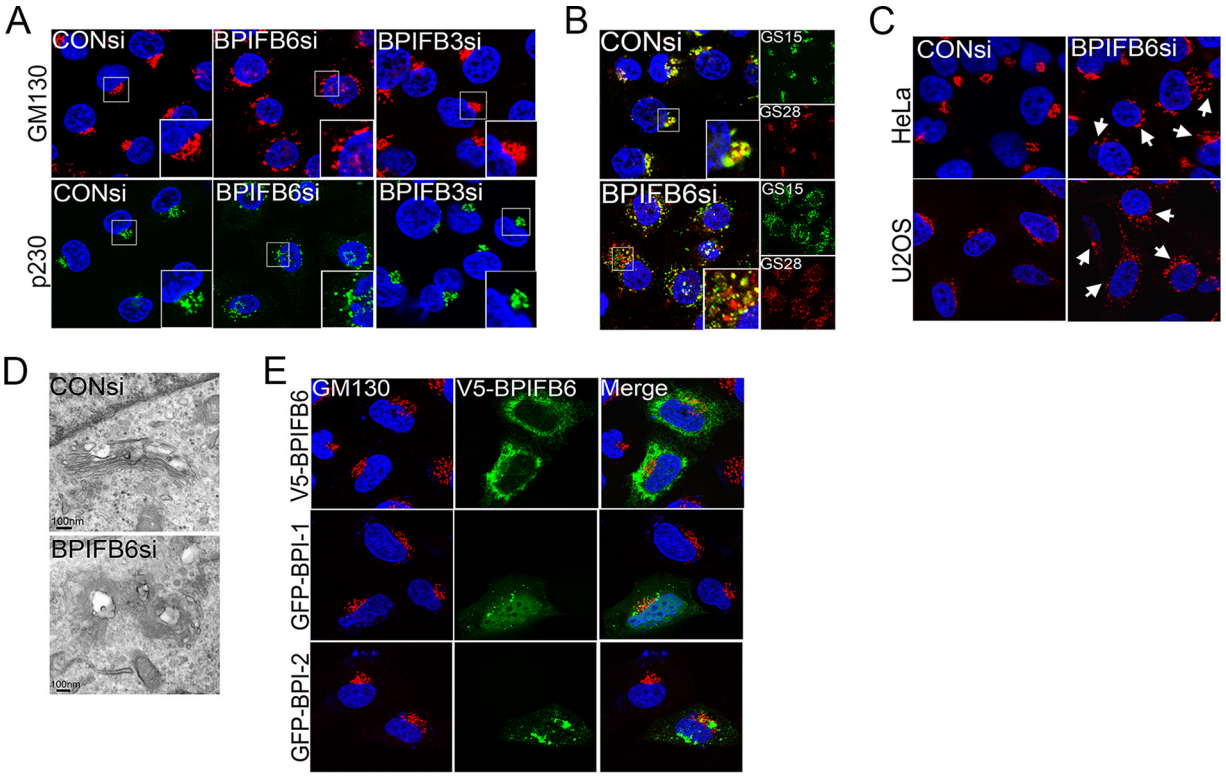

FIG 5 Silencing of BPIFB6 induces Golgi complex fragmentation. (A) Confocal microscopy for GM130 (red) or p230 (green) in HBMECs transfected with control siRNA (scrambled [CONsi]) or BPIFB6si. At bottom right is shown a 2× magnification of the area shown in the white box. (B) Confocal microscopy for GS15 (green) and GS28 (red) in HBMECs transfected with CONsi or BPIFB6si. At bottom right is shown a 2× magnification of the area shown in the white box. (C) Confocal microscopy for GM130 (red) in HeLa (top row) or U2OS (bottom row) cells transfected with CONsi or BPIFB6si. White areas denote fragmented Golgi complex. (D) Transmission electron micrographs of Golgi complexes in HBMECs transfected with CONsi or BPIFB6si. The scale bar at the bottom left is 100 nm. (E) Confocal microscopy for GM130 (red) and V5 (green, top row) or GFP (middle and bottom rows) in U2OS cells transfected with full-length V5-BPIFB6 (top row) or GFP-fused BPI domains of BPIFB6 (BPI-1 in the middle row and BPI-2 in the bottom row).

localize with ER-localized Sec61β. We found that mutants with both single (C164S and C199A for BPIFB3 and C137S and C174S for BPIFB6) and double mutations of these sites retained their ability to localize to the ER, suggesting that the lipid-binding abilities of BPIFB3 and BPIFB6 do not lead to their ER localization (Fig. 3D and E).

Silencing of BPIFB6 expression induces alterations in anterograde and retrograde trafficking. Our previous work showed that RNAi-mediated silencing of BPIFB3 induced significant increases in the levels of autophagy, which correlated with the appearance of enlarged lysosomes (15). However, silencing of BPIFB6 has no effect on autophagy (15), suggesting that decreases in enterovirus replication induced by depletion of BPIFB6 are not the result of alterations in the autophagic pathway. Given that all enteroviruses rely heavily on the secretory pathway to facilitate their replication, we determined whether silencing of BPIFB6 impacted the vesicles and/or organelles associated with this pathway. We found that silencing of BPIFB6 expression induced dramatic alterations in the localization of vesicles associated with both anterograde (as assessed by the localization of Sec31A) and retrograde (as assessed by the localization of βCOP) trafficking (Fig. 4A, bottom panel). In contrast, silencing of BPIFB3 had no effect on either Sec31A or βCOP (Fig. 4A, middle panel). In addition, we found that silencing of BPIFB6 expression also induced pronounced mislocalization of the ERGIC marker ERGIC-53 (Fig. 4B). Collectively, these data point to a direct role for BPIFB6, but not BPIFB3, in secretory pathway trafficking.

Silencing of BPIFB6 alters Golgi complex morphology. Given that we observed dramatic alterations in anterograde and retrograde trafficking in cells transfected with BPIFB6 siRNA, we next assessed the impact of this treatment on Golgi complex morphology. Consistent with the dramatic changes in vesicular transport induced by RNAi-mediated silencing of BPIFB6, we found that suppression of BPIFB6 expression led to dramatic changes in the morphology of the Golgi complex, as assessed by the pronounced mislocalization of the *cis*-Golgi marker GM130 and the *trans*-Golgi marker p230 to vesicular structures (Fig. 5A). In contrast, silencing of BPIFB3 had no effect on the localization of either GM130 or p230, which both localized to juxtanuclear structures similar to control cells (Fig. 5A). In addition to the relocalization of *cis*- and *trans*-Golgi markers, we also found that silencing of BPIFB6 led to a dramatic relocalization of the intra-Golgi v-SNAREs GS15 and GS28 to vesicular structures localized throughout the cytoplasm (Fig. 5B) and that silencing of BPIFB6 expression in multiple cell types, including HeLa and U2OS cells, also induced Golgi fragmentation (Fig. 5C), suggesting that BPIFB6 functions as a regulator of secretory pathway trafficking in a pan-cell-type manner.

Ultrastructurally, RNAi-mediated silencing of BPIFB6 led to the formation of dilated cisternae and Golgi complex fragmenta-

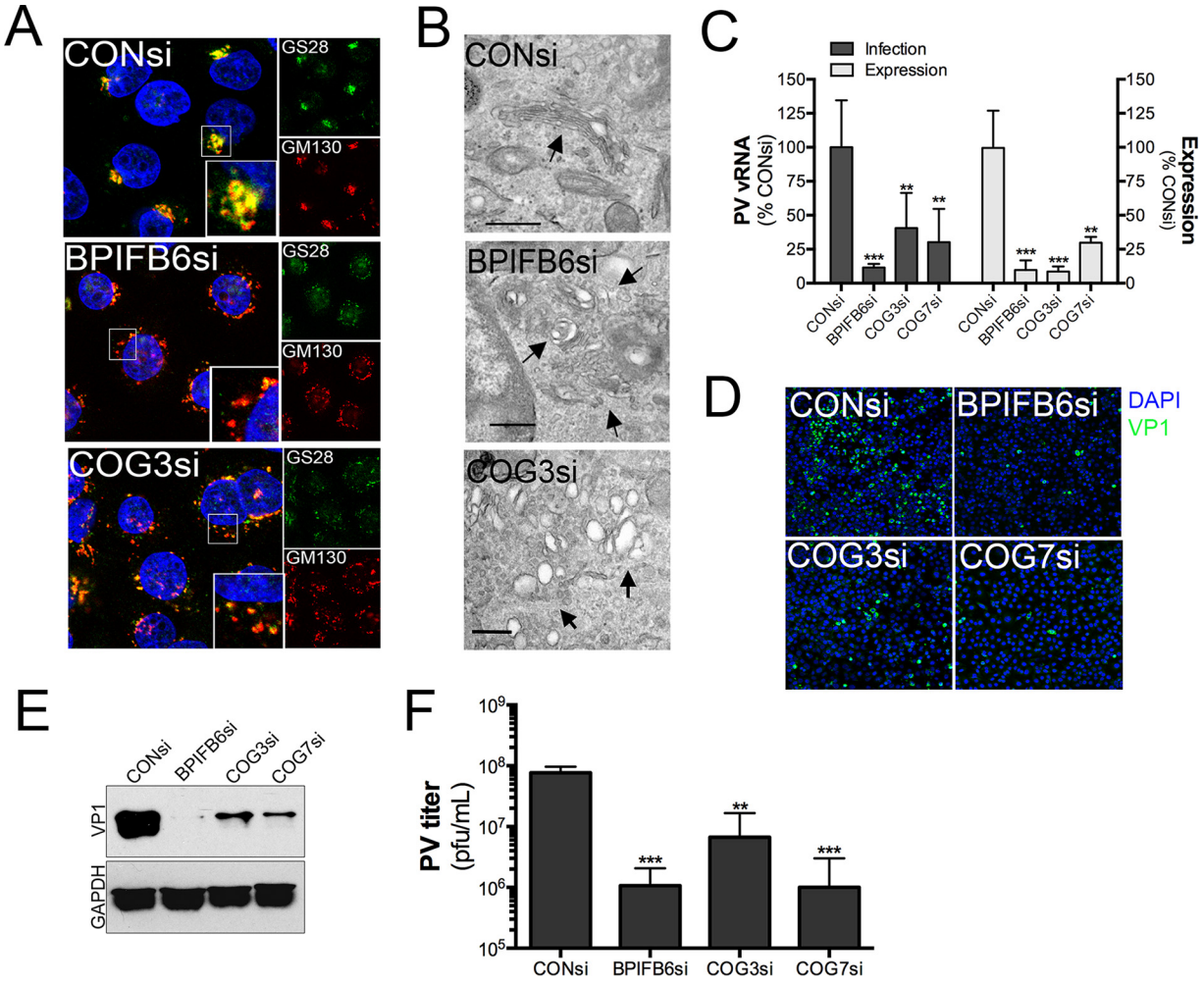

FIG 6 Silencing of COG complex components inhibits enterovirus replication. (A) Confocal microscopy for GS28 (green) and GM130 (red) in HBMECs transfected with control siRNA (scrambled [CONsi]), BPIFB6si, or COG3si. At bottom right is shown a 2× magnification of the area shown in the white box. (B) Transmission electron micrographs of Golgi complexes in HBMECs transfected with CONsi, BPIFB6si, or COG3si. The scale bar at the bottom left is 100 nm. (C) HBMECs were transfected with siRNAs against BPIFB6, COG3, or CO73 (or control scrambled siRNA) and infected with PV (1 PFU/cell) ~48 h later. Infections (left) and the level of expression (right) were quantified by RT-qPCR. Data are shown as a percentage of change from control siRNA (CONsi). (D) Confocal microscopy for PV viral RNA (green) in HBMECs transfected with CONsi, BPIFB6si, COG3si, or COG7si and infected with PV for ~16 h. (E) Immunoblots for VP1 (top) and GAPDH (bottom) in HBMECs transfected with CONsi, BPIFB6si, COG3si, or COG7si and infected with PV for ~16 h. (F) Viral titers (PFU per cell) in in HBMECs transfected with CONsi, BPIFB6si, COG3si, or COG7si and infected with PV for ~16 h. In panels A and D, DAPI-stained nuclei are shown in blue. In panels C and F, data are shown as means ± standard deviations (**, $P < 0.05$; ***, $P < 0.001$).

tion (Fig. 5D). However, unlike silencing of BPIFB6, we found that overexpression of BPIFB6, or its individual BPI domains, had no effect on Golgi complex morphology as assessed by GM130 localization (Fig. 5E).

Silencing of COG complex components reduces enterovirus infection. The COG complex regulates retrograde transport, and its depletion by RNAi induces pronounced Golgi complex fragmentation due to destabilization of the cisternal region of the Golgi complex (9). We found that the extent of Golgi complex fragmentation induced by BPIFB6 depletion was similar to that induced by depletion of COG3, an essential component of the COG complex, as assessed by immunofluorescence microscopy (Fig. 6A) and transmission electron microscopy (TEM) (Fig. 6B).

Given that depletion of BPIFB6 drastically reduced enterovirus infection and led to pronounced alterations in secretory pathway trafficking, we reasoned that depletion of members of the COG complex would induce similar effects. Indeed, we found that silencing of either COG3 or COG7, a necessary component for COG complex assembly (28), also reduced PV replication, which correlated with reduced production of vRNA (Fig. 6C and D), viral protein production (Fig. 6E), and ~1-log loss of PV titers (Fig. 6F).

DISCUSSION

Very little is known regarding the cellular functions of members of the BPIFB family. Whereas our previous work showed that BPIFB3 regulates autophagy and serves as a negative regulator of CVB replication (15), we show here that BPIFB6 controls secretory pathway trafficking and Golgi complex morphology to serve as a positive regulator of enterovirus infection. Collectively, our studies have identified distinct functions for members of the

BPIFB family, which serve opposing roles in the regulation of enterovirus replication.

The lipid binding capabilities of BPIFB3 and BPIFB6 suggest that this activity influences their role in regulating distinct cellular processes, particularly given that the expression and correct localization of lipids within the ER are associated with both autophagy and secretory pathway trafficking. Our results show that both BPI domains of BPIFB6 bind to distinct lipids—PA, PS, PI(4)P, cardiolipin, and sulfatide, with the strongest binding to PA, PS, and PI(4)P. Interestingly, many of these lipids have been shown to play important roles in the regulation of secretory pathway trafficking. PA is enriched in the ER (29), where it localizes to ER exit sites (30) and is required for maintaining the structural integrity of the Golgi complex by facilitating the budding of secretory vesicles (31). Likewise, PI(4)P is also enriched at ER exit sites, where it promotes the export of COPII-coated vesicles and promotes the SNARE-mediated fusion of COPII-coated vesicles to the Golgi complex (32, 33). Furthermore, PI(4)P is enriched in enterovirus replication complexes, where it interacts with the virally encoded polymerase $3D^{pol}$ (34).

Lipid transfer between the ER and other cellular organelles and between opposing membranes within the ER is essential to deliver lipids to their proper cellular locations. The transport of lipids within the ER is accomplished by several different mechanisms, including the direct delivery of lipids by various lipid transfer proteins (LTPs), which utilize hydrophobic pockets to transport lipids through an aqueous phase (reviewed in reference 35). Given that BPIFB6 and BPIFB3 bind to select lipids, it is possible that they facilitate some aspect of lipid transfer either between intra-ER membranes or between the ER and other organelles and/or vesicles. This is supported by our data showing that BPIFB3 and BPIFB6 localize exclusively to the ER and do not exhibit any localization to non-ER compartments. However, despite their restricted expression to the ER, silencing of either BPIFB3 or BPIFB6 has impacts on host cell processes such as autophagy and Golgi complex morphology, despite their lack of localization to either autophagosomes (15) or the Golgi complex.

We showed previously that BPIFB3 functions as a negative regulator of enterovirus replication in a virus-specific manner (15). Whereas silencing of BPIFB3 enhanced CVB replication, this treatment had no effect on PV replication. In contrast, we show here that BPIFB6 specifically regulated enterovirus replication from several species groups, and its silencing significantly reduces the replication of CVB, PV, E11, and EV71. Unlike autophagy, which may facilitate unique aspects of enterovirus replication in a virus-specific manner, such as in virus reliance on flux through the autophagic pathway (36, 37), all enteroviruses rely on intact secretory pathway trafficking to facilitate their replicative life cycles. Enteroviruses utilize ER exit sites to form tubular structures that extend into the cytoplasm to anchor the viral replication machinery on the cytoplasmic membrane of the ER (34, 38). The formation of enterovirus replication organelles also specifically requires COPI (39–41), which is recruited to replication complexes via the inhibition of the activity of the Arf1 GTPase by the virally encoded 3A protein (42, 43). Thus, even subtle alterations in any aspect of secretory pathway trafficking could have profound effects on the formation of enterovirus replication organelles, thus inhibiting infection at a very early time point in the virus life cycle. Given that silencing of BPIFB6 induces dramatic alterations in anterograde and retrograde trafficking, as well as pronounced Golgi complex fragmentation, it is not surprising that enterovirus replication would be impacted by this treatment. Consistent with its role in regulating these pathways, we found that silencing of BPIFB6 prevented the formation of CVB replication organelles.

Here, we report on the cellular function of a member of the BPIFB family, BPIFB6, in the regulation of secretory pathway trafficking and Golgi complex morphology. In addition, we show that BPIFB6 functions as a positive regulator of enterovirus replication via its regulation of the secretory pathway. Given that we previously showed that BPIFB3 functions as a proviral regulator of enterovirus replication in a virus-specific manner through the autophagic pathway, our results identify distinct BPIFB family members in the regulation of specific host cell pathways and as host cell regulators of viral replication.

ACKNOWLEDGMENTS

We thank Kwang Sik Kim (Johns Hopkins University) for human brain microvascular endothelial cells (HBMECs) and Donna Stolz (University of Pittsburgh) for assistance with electron microscopy.

This project was supported by NIH R01-AI081759 (C.B.C), T32 AI060525 (N.J.L.), and a Burroughs Wellcome Investigators in the Pathogenesis of Infectious Disease Award (C.B.C).

FUNDING INFORMATION

This work, including the efforts of Carolyn B. Coyne, was funded by HHS | NIH | National Institute of Allergy and Infectious Diseases (NIAID) (R01-AI081759). This work, including the efforts of Nicholas J. Lennemann, was funded by HHS | NIH | National Institute of Allergy and Infectious Diseases (NIAID) (T32-AI060525). This work, including the efforts of Carolyn B. Coyne, was funded by Burroughs Wellcome Fund (BWF) (PATH).

REFERENCES

1. **Ungar D, Oka T, Brittle EE, Vasile E, Lupashin VV, Chatterton JE, Heuser JE, Krieger M, Waters MG.** 2002. Characterization of a mammalian Golgi-localized protein complex, COG, that is required for normal Golgi morphology and function. J Cell Biol **157:**405–415. http://dx.doi.org/10.1083/jcb.200202016.
2. **Walter DM, Paul KS, Waters MG.** 1998. Purification and characterization of a novel 13 S hetero-oligomeric protein complex that stimulates in vitro Golgi transport. J Biol Chem **273:**29565–29576. http://dx.doi.org/10.1074/jbc.273.45.29565.
3. **VanRheenen SM, Cao X, Lupashin VV, Barlowe C, Waters MG.** 1998. Sec35p, a novel peripheral membrane protein, is required for ER to Golgi vesicle docking. J Cell Biol **141:**1107–1119. http://dx.doi.org/10.1083/jcb.141.5.1107.
4. **VanRheenen SM, Cao X, Sapperstein SK, Chiang EC, Lupashin VV, Barlowe C, Waters MG.** 1999. Sec34p, a protein required for vesicle tethering to the yeast Golgi apparatus, is in a complex with Sec35p. J Cell Biol **147:**729–742. http://dx.doi.org/10.1083/jcb.147.4.729.
5. **Suvorova ES, Duden R, Lupashin VV.** 2002. The Sec34/Sec35p complex, a Ypt1p effector required for retrograde intra-Golgi trafficking, interacts with Golgi SNAREs and COPI vesicle coat proteins. J Cell Biol **157:**631–643. http://dx.doi.org/10.1083/jcb.200111081.
6. **Shestakova A, Suvorova E, Pavliv O, Khaidakova G, Lupashin V.** 2007. Interaction of the conserved oligomeric Golgi complex with t-SNARE Syntaxin5a/Sed5 enhances intra-Golgi SNARE complex stability. J Cell Biol **179:**1179–1192. http://dx.doi.org/10.1083/jcb.200705145.
7. **Farkas RM, Giansanti MG, Gatti M, Fuller MT.** 2003. The Drosophila Cog5 homologue is required for cytokinesis, cell elongation, and assembly of specialized Golgi architecture during spermatogenesis. Mol Biol Cell **14:**190–200. http://dx.doi.org/10.1091/mbc.E02-06-0343.
8. **Belloni G, Sechi S, Riparbelli MG, Fuller MT, Callaini G, Giansanti MG.** 2012. Mutations in Cog7 affect Golgi structure, meiotic cytokinesis and sperm development during Drosophila spermatogenesis. J Cell Sci **125:**5441–5452. http://dx.doi.org/10.1242/jcs.108878.
9. **Zolov SN, Lupashin VV.** 2005. Cog3p depletion blocks vesicle-mediated

Golgi retrograde trafficking in HeLa cells. J Cell Biol **168:**747–759. http://dx.doi.org/10.1083/jcb.200412003.
10. **Irurzun A, Perez L, Carrasco L.** 1992. Involvement of membrane traffic in the replication of poliovirus genomes: effects of brefeldin A. Virology **191:**166–175. http://dx.doi.org/10.1016/0042-6822(92)90178-R.
11. **Maynell LA, Kirkegaard K, Klymkowsky MW.** 1992. Inhibition of poliovirus RNA synthesis by brefeldin A. J Virol **66:**1985–1994.
12. **Doedens JR, Kirkegaard K.** 1995. Inhibition of cellular protein secretion by poliovirus proteins 2B and 3A. EMBO J **14:**894–907.
13. **Beske O, Reichelt M, Taylor MP, Kirkegaard K, Andino R.** 2007. Poliovirus infection blocks ERGIC-to-Golgi trafficking and induces microtubule-dependent disruption of the Golgi complex. J Cell Sci **120:**3207–3218. http://dx.doi.org/10.1242/jcs.03483.
14. **van Kuppeveld FJ, de Jong AS, Melchers WJ, Willems PH.** 2005. Enterovirus protein 2B po(u)res out the calcium: a viral strategy to survive? Trends Microbiol **13:**41–44. http://dx.doi.org/10.1016/j.tim.2004.12.005.
15. **Delorme-Axford E, Morosky S, Bomberger J, Stolz DB, Jackson WT, Coyne CB.** 2014. BPIFB3 regulates autophagy and coxsackievirus B replication through a noncanonical pathway independent of the core initiation machinery. mBio **5:**e02147-14. http://dx.doi.org/10.1128/mBio.02147-14.
16. **Bingle CD, Bingle L, Craven CJ.** 2011. Distant cousins: genomic and sequence diversity within the BPI fold-containing (BPIF)/PLUNC protein family. Biochem Soc Trans **39:**961–965. http://dx.doi.org/10.1042/BST0390961.
17. **Andrault JB, Gaillard I, Giorgi D, Rouquier S.** 2003. Expansion of the BPI family by duplication on human chromosome 20: characterization of the RY gene cluster in 20q11.21 encoding olfactory transporters/antimicrobial-like peptides. Genomics **82:**172–184. http://dx.doi.org/10.1016/S0888-7543(03)00102-2.
18. **Stins MF, Badger J, Sik Kim K.** 2001. Bacterial invasion and transcytosis in transfected human brain microvascular endothelial cells. Microb Pathog **30:**19–28. http://dx.doi.org/10.1006/mpat.2000.0406.
19. **Coyne CB, Bozym R, Morosky SA, Hanna SL, Mukherjee A, Tudor M, Kim KS, Cherry S.** 2011. Comparative RNAi screening reveals host factors involved in enterovirus infection of polarized endothelial monolayers. Cell Host Microbe **9:**70–82. http://dx.doi.org/10.1016/j.chom.2011.01.001.
20. **Coyne CB, Kim KS, Bergelson JM.** 2007. Poliovirus entry into human brain microvascular cells requires receptor-induced activation of SHP-2. EMBO J **26:**4016–4028. http://dx.doi.org/10.1038/sj.emboj.7601831.
21. **Delorme-Axford E, Donker RB, Mouillet JF, Chu T, Bayer A, Ouyang Y, Wang T, Stolz DB, Sarkar SN, Morelli AE, Sadovsky Y, Coyne CB.** 2013. Human placental trophoblasts confer viral resistance to recipient cells. Proc Natl Acad Sci U S A **110:**12048–12053. http://dx.doi.org/10.1073/pnas.1304718110.
22. **Saito K, Chen M, Bard F, Chen S, Zhou H, Woodley D, Polischuk R, Schekman R, Malhotra V.** 2009. TANGO1 facilitates cargo loading at endoplasmic reticulum exit sites. Cell **136:**891–902. http://dx.doi.org/10.1016/j.cell.2008.12.025.
23. **Livak KJ, Schmittgen TD.** 2001. Analysis of relative gene expression data using real-time quantitative PCR and the $2^{-\Delta\Delta CT}$ method. Methods **25:**402–408. http://dx.doi.org/10.1006/meth.2001.1262.
24. **Shibata Y, Shemesh T, Prinz WA, Palazzo AF, Kozlov MM, Rapoport TA.** 2010. Mechanisms determining the morphology of the peripheral ER. Cell **143:**774–788. http://dx.doi.org/10.1016/j.cell.2010.11.007.
25. **Rismanchi N, Soderblom C, Stadler J, Zhu PP, Blackstone C.** 2008. Atlastin GTPases are required for Golgi apparatus and ER morphogenesis. Hum Mol Genet **17:**1591–1604. http://dx.doi.org/10.1093/hmg/ddn046.
26. **Beamer LJ, Carroll SF, Eisenberg D.** 1997. Crystal structure of human BPI and two bound phospholipids at 2.4 angstrom resolution. Science **276:**1861–1864. http://dx.doi.org/10.1126/science.276.5320.1861.
27. **Horwitz AH, Leigh SD, Abrahamson S, Gazzano-Santoro H, Liu PS, Williams RE, Carroll SF, Theofan G.** 1996. Expression and characterization of cysteine-modified variants of an amino-terminal fragment of bactericidal/permeability-increasing protein. Protein Expr Purif **8:**28–40. http://dx.doi.org/10.1006/prep.1996.0071.
28. **Loh E, Hong W.** 2004. The binary interacting network of the conserved oligomeric Golgi tethering complex. J Biol Chem **279:**24640–24648. http://dx.doi.org/10.1074/jbc.M400662200.
29. **Struck DK, Pagano RE.** 1980. Insertion of fluorescent phospholipids into the plasma membrane of a mammalian cell. J Biol Chem **255:**5404–5410.
30. **Shimoi W, Ezawa I, Nakamoto K, Uesaki S, Gabreski G, Aridor M, Yamamoto A, Nagahama M, Tagaya M, Tani K.** 2005. p125 is localized in endoplasmic reticulum exit sites and involved in their organization. J Biol Chem **280:**10141–10148. http://dx.doi.org/10.1074/jbc.M409673200.
31. **Siddhanta A, Backer JM, Shields D.** 2000. Inhibition of phosphatidic acid synthesis alters the structure of the Golgi apparatus and inhibits secretion in endocrine cells. J Biol Chem **275:**12023–12031. http://dx.doi.org/10.1074/jbc.275.16.12023.
32. **Lorente-Rodriguez A, Barlowe C.** 2011. Requirement for Golgi-localized PI(4)P in fusion of COPII vesicles with Golgi compartments. Mol Biol Cell **22:**216–229. http://dx.doi.org/10.1091/mbc.E10-04-0317.
33. **Blumental-Perry A, Haney CJ, Weixel KM, Watkins SC, Weisz OA, Aridor M.** 2006. Phosphatidylinositol 4-phosphate formation at ER exit sites regulates ER export. Dev Cell **11:**671–682. http://dx.doi.org/10.1016/j.devcel.2006.09.001.
34. **Hsu NY, Ilnytska O, Belov G, Santiana M, Chen YH, Takvorian PM, Pau C, van der Schaar H, Kaushik-Basu N, Balla T, Cameron CE, Ehrenfeld E, van Kuppeveld FJ, Altan-Bonnet N.** 2010. Viral reorganization of the secretory pathway generates distinct organelles for RNA replication. Cell **141:**799–811. http://dx.doi.org/10.1016/j.cell.2010.03.050.
35. **Lev S.** 2012. Nonvesicular lipid transfer from the endoplasmic reticulum. Cold Spring Harb Perspect Biol **4:**a013300. http://dx.doi.org/10.1101/cshperspect.a013300.
36. **Richards AL, Jackson WT.** 2012. Intracellular vesicle acidification promotes maturation of infectious poliovirus particles. PLoS Pathog **8:**e1003046. http://dx.doi.org/10.1371/journal.ppat.1003046.
37. **Wong J, Zhang J, Si X, Gao G, Mao I, McManus BM, Luo H.** 2008. Autophagosome supports coxsackievirus B3 replication in host cells. J Virol **82:**9143–9153. http://dx.doi.org/10.1128/JVI.00641-08.
38. **Limpens RW, van der Schaar HM, Kumar D, Koster AJ, Snijder EJ, van Kuppeveld FJ, Barcena M.** 2011. The transformation of enterovirus replication structures: a three-dimensional study of single- and double-membrane compartments. mBio **2:**e00166-11. http://dx.doi.org/10.1128/mBio.00166-11.
39. **Gazina EV, Mackenzie JM, Gorrell RJ, Anderson DA.** 2002. Differential requirements for COPI coats in formation of replication complexes among three genera of Picornaviridae. J Virol **76:**11113–11122. http://dx.doi.org/10.1128/JVI.76.21.11113-11122.2002.
40. **Cherry S, Kunte A, Wang H, Coyne C, Rawson RB, Perrimon N.** 2006. COPI activity coupled with fatty acid biosynthesis is required for viral replication. PLoS Pathog **2:**e102. http://dx.doi.org/10.1371/journal.ppat.0020102.
41. **Richards AL, Soares-Martins JA, Riddell GT, Jackson WT.** 2014. Generation of unique poliovirus RNA replication organelles. mBio **5:**e00833-13. http://dx.doi.org/10.1128/mBio.00833-13.
42. **Wessels E, Duijsings D, Niu TK, Neumann S, Oorschot VM, de Lange F, Lanke KH, Klumperman J, Henke A, Jackson CL, Melchers WJ, van Kuppeveld FJ.** 2006. A viral protein that blocks Arf1-mediated COP-I assembly by inhibiting the guanine nucleotide exchange factor GBF1. Dev Cell **11:**191–201. http://dx.doi.org/10.1016/j.devcel.2006.06.005.
43. **Belov GA, Fogg MH, Ehrenfeld E.** 2005. Poliovirus proteins induce membrane association of GTPase ADP-ribosylation factor. J Virol **79:**7207–7216. http://dx.doi.org/10.1128/JVI.79.11.7207-7216.2005.